PCCP

PAPER

View Article Online
View Journal | View Issue

Cite this: *Phys. Chem. Chem. Phys.*, 2019, **21**, 21317

Highly fluorescent hybrid Au/Ag nanoclusters stabilized with poly(ethylene glycol)- and zwitterion-modified thiolate ligands†

Dinesh Mishra,[a] Sisi Wang,[a] Zhicheng Jin,[a] Yan Xin,[b] Eric Lochner[c] and Hedi Mattoussi*[a]

Received 2nd July 2019,
Accepted 9th September 2019

DOI: 10.1039/c9cp03723c

rsc.li/pccp

We report a simple strategy to grow highly fluorescing, near-infrared-emitting nanoclusters (NCs) made of bimetallic Au/Ag cores, surface capped with a mixture of triphenylphosphine and various monothiol ligands. The ligands include short chain aliphatic monothiols, which yields hydrophobic NCs, and poly(ethylene glycol)- or zwitterion-appended monothiols, which yield NCs that are readily dispersible in buffer media. The reaction uses well-defined triphenylphosphine-protected Au_{11} clusters (as precursors) that are reacted with Ag(I)–thiolate complexes. The prepared materials are small (diameter <2 nm, as characterized by TEM) with emission peak at 730–760 nm and long lifetime ($\sim$8–12 μs). The quantum yield measured for these materials in both hydrophobic and hydrophilic dispersions is $\sim$40%. High-magnification dark field STEM and X-ray photoelectron spectroscopy measurements show the presence of both metal atoms in the core, with measured binding energies that agree with reported values for nanocluster materials. The NIR emission combined with high quantum yield, small size, colloidal stability in buffer media and ease of surface functionalization afforded by the coating, make these materials suitable for investigating fundamental questions and potentially useful for biological sensing and imaging applications.

Introduction

Use of luminescent nanomaterials in applications ranging from opto-electronics to sensing and imaging has gained tremendous interest.[1,2] These include luminescent quantum dots (QDs),[3–5] lanthanide nanoparticles,[6,7] carbon dots[8] and noble metal nanoclusters (NCs).[9–12] Due to their small size, broad range of emissions and photo-stability, luminescent metal nanoclusters are promising candidates for use in such applications. In addition, these materials have generated much interest from scientists across different disciplines to understand their unique fundamental properties, including magic size formation, spectroscopic properties, importance of the capping ligand and its ability to affect the absorption and emission properties of the prepared materials.[1,13–15] To expand the potential utility of these materials, it is necessary to grow highly fluorescent nanoclusters with control over their stoichiometry, surface properties and colloidal stability in a wide range of solution conditions. Broadly, growth of nanoclusters can be classified into two categories: (i) direct reduction of metal precursors (*e.g.*, Au(III) or Ag(I) salts),[12,16–19] and (ii) transformation of grown metal clusters into new nanoclusters *via* ligand exchange, or reaction with metal thiolate complexes.[13,20–23]

The first route refers to the reduction of metal precursors (or metal salts) in the presence of suitable coordinating ligands, yielding ligand-stabilized nanoclusters. This can be achieved by chemical reduction, photo-reduction, or thermal reduction.[2,16,24–27] Ligands used include triphenylphosphine, thiolate molecules, peptides, protein scaffolds as well as DNA templates. Depending on the nature of the ligand used, the structure and optical properties of the resulting nanoclusters differ widely. Both mono-metallic and bimetallic (or alloy) nanoclusters can be prepared using the direct reduction route.[28–32] However, controlling the size and composition of the nanoclusters using chemical reduction is tedious and sometimes difficult to achieve. Among the plethora of synthetic methods reported to-date using this direct reduction, only a few of those have successfully been used to grow homogenous nanoclusters.

Core transformation of small clusters, in comparison, is an attractive route to grow atomically precise nanoclusters with

[a] *Department of Chemistry and Biochemistry, Florida State University, 95 Chieftan Way, Tallahassee, FL 32306, USA. E-mail: hmattoussi@fsu.edu*
[b] *National High Magnetic Field Laboratory, Florida State University, 1800 E. Paul Dirac Drive, Tallahassee, Florida, 32310, USA*
[c] *CMMP, Department of Physics, Florida State University, 77 Chieftan Way, Tallahassee, FL 32306, USA*

† Electronic supplementary information (ESI) available: Additional information including NMR spectra of the ligands, absorption data for the PPh_3-capped Au_{11} NCs, azide, amine and carboxy functionalization of the nanoclusters. See DOI: 10.1039/c9cp03723c

reproducible photo-physical properties. The idea builds on initial work by Teo and co-workers who explored among others the assembly of larger magic size nanoclusters, including Au_{25} and Au_{37} cores, starting from a 13-atom cluster as building block; in these organized assemblies (referred to as "clusters of clusters") an atom is shared between two adjacent building blocks.[33,34] More recently, the approach has been exploited by other groups, as a means of preparing fluorescent materials with promising properties. For example, ligand exchange of triphenylphosphine-stabilized undecagold (Au_{11}) clusters with thiolate ligands resulted in the formation of bi-icosahedral nanoclusters with the stoichiometry/composition $[Au_{25}(PPh_3)_{10}(SC_2H_5)_5Cl_2]^{2+}$.[20,35] However, nanoclusters with Au_{25} cores prepared using this route are essentially non-luminescent (*i.e.*, they exhibit PL quantum yield of ~0.1–0.2%). Nonetheless, recent studies have shown that it is possible to dope Au_{25} nanoclusters with other metal thiolate complexes, a process commonly known as metal atom exchange.[21] In one report, Jin and co-workers detailed the preparation of bimetallic $[Au_{25-x}Ag_x(PPh_3)_{10}(SR)_5Cl_2]^{2+}$ NCs by reacting $[Au_{11}(PPh_3)_8Cl_2]^+$ cores with Ag(I)–thiolate complexes.[23] They further showed that Ag(I)-complexes formed with aromatic and short aliphatic thiols (as ligands) promote the formation of nanoclusters capped with mixed ligand composition. These NCs exhibited a large enhancement (~200-fold) in the fluorescence properties, compared to Au_{25} NCs; the bimetallic NCs have a fluorescence quantum yield (QY) of ~40%. Furthermore, they were able to crystallize these NCs and characterize them using X-ray diffraction measurements. The X-ray data were exploited to propose an atomic arrangement in the NCs, where the silver atoms occupy the core of the bi-icosahedral structure, surrounded by the gold atoms. Additionally, the proposed structure indicates that the Au atoms are coordinated to the phosphine ligands and the Ag atoms are bridged by thiol ligands, with the two chlorine atoms being attached to the opposite terminal silver-substituted atoms of the bi-icosahedron.[23]

Surface coating and functionalization of these metallic nanocrystals, as a means of tuning their solubility and coupling them to target molecules, has been pursued by various groups. This approach requires access to functional ligands that also present metal-coordinating motifs. Our group has developed several modular ligands that are appended with a poly(ethylene glycol) block or a zwitterion group, and applied them for the capping of a variety of colloidal nanocrystals including luminescent quantum dots and plasmonic nanostructures.[36–39] We found that these amphiphilic ligands allow great flexibility for dispersing these nanomaterials in conditions ranging from organic solvents to buffer and protein-rich media. Additionally, ligands bearing the zwitterion motif provide water dispersible nanocrystals that are compact in size.[40,41]

Here, we build on the above developments to grow highly luminescent bimetallic Au/Ag NCs that are surface-capped with either a set of hydrophobic ligands (*i.e.*, alkyl thiols), or alkyl thiol appended with hydrophilic motifs, including a poly(ethylene glycol), PEG, block and a zwitterion group. We further characterize the prepared materials using optical absorption, fluorescence spectroscopy, transmission electron microcopy (TEM), X-ray photoelectron spectroscopy (XPS), as well as Fourier transform infrared (FT-IR) spectroscopy measurements. This growth strategy also allows the introduction of terminal groups with distinct functionalities on the NCs, such as $-OCH_3$, $-N_3$, $-NH_2$ and –COOH.

Experimental section

Materials

1-Propanethiol (99%), 3-mercaptopropionic acid (99%), 1-hexanethiol (95%), 1-dodecanethiol (98%), 11-bromoundecanoic acid (95%), triphenylphosphine (99%), *N*,*N*-dimethyl-1,3-propanediamine (99%), 4-(*N*,*N*-dimethylamino)pyridine (99%), triethylamine (Et_3N), *N*,*N*′-dicyclohexylcarbodiimide (DCC), poly(ethylene glycol) (average MW = 600), poly(ethylene glycol) methyl ether (average MW = 750), sodium borohydride (99.99%, granular), tetrachloroauric acid trihydrate (99.9%) and potassium thioacetate (98%) were purchased from Sigma Aldrich (St Louis, MO). Silver nitrate (99.9%), 1,3-propanesultone (99%) and 1,1′-carbonyldiimidazole (CDI) (97%) were purchased from Alfa-Aesar (Wardhill, MA). The solvents used in this study (ethanol, dimethyl formamide, chloroform, ethyl acetate, *etc.*) were also purchased from Sigma-Aldrich and used as purchased. Column purification chromatography of the synthesized ligands was performed using silica gel (60 Å, 230–400 mesh, from Bodman Industries, Aston, PA). PD10 columns were purchased from Lumiprobe (Hallandale Beach, FL).

Instrumentation, data collection and analyses

The UV-vis absorption measurements were carried out using a Shimadzu 2450 UV-vis absorption spectrophotometer (Columbia, MD), while the fluorescence emission profiles and excitation spectra were collected using a Fluorolog-3 spectrometer equipped with a fast TBX PMT detector, from Horiba Jobin Yvon Inc. (Edison, NJ).

The fluorescence quantum yield measurements were carried out using a Quantaurus absolute PL quantum yield spectrometer (C11347) from Hamamatsu (Bridgewater, NJ); the excitation wavelength is at 485 nm. The setup measures the integrated signal over the fluorescence spectrum, which is then normalized with respect to the excitation profile. The QY values of the NCs were extracted from the intensities of the signals emitted, I(Em), and absorbed, I(Abs), by the sample using the equation:

$$\Phi = \frac{I(\mathrm{Em})}{I(\mathrm{Abs})} = \frac{\int_{\lambda_3}^{\lambda_4}\left(\frac{\lambda}{hc}\right) \times \left\{I_S^{\text{T-Corr}}(\lambda) - I_R^{\text{T-Corr}}(\lambda)\right\}\mathrm{d}\lambda}{\int_{\lambda_1}^{\lambda_2}\left(\frac{\lambda}{hc}\right) \times \left\{I_R^{\text{T-Corr}}(\lambda) - I_S^{\text{T-Corr}}(\lambda)\right\}\mathrm{d}\lambda} \quad (1)$$

where h and c designate the Planck constant and speed of light, respectively. The wavelength intervals $[\lambda_1, \lambda_2]$ and $[\lambda_3, \lambda_4]$ designate the range limits for the excitation profile and sample emission, respectively. $I_R^{\text{T-cor}}(\lambda) = I_R(\lambda)/T(\lambda)$ and $I_S^{\text{T-cor}}(\lambda) = I_S(\lambda)/T(\lambda)$ are the corrected intensities of the excitation and sample emission profiles, respectively, accounting for the transmission of the sample/reference, $T(\lambda)$. $I_R(\lambda)$ and $I_S(\lambda)$ refer to the intensity of the excitation source and sample emission (which also

includes a small contribution from the excitation signal). We used dilute samples with low absorbance values (~ 0.1) in order to minimize the effects of self-absorption.

The time-resolved (TR) fluorescence measurements were carried out using two systems. The first is an Edinburgh FLS980 fluorescence spectrometer, where the emission decay traces were acquired using a pulsed excitation at 485 nm from a 60 W microsecond flashlamp (pulse width <2.5 μs), repetition rate at a 100 Hz, and a multichannel scaling (MCS) acquisition mode. The PL signal was passed through a long pass filter, then a single grating Czerny–Turner monochromator (1800 groove per mm, 500 nm blaze), and detected using a Peltier-cooled Hamamatsu R928 photomultiplier tube. The second set of TR fluorescence decays were collected and analyzed using a Time Correlation Single Photon Counting (TCSPC) system mounted on the same Fluorolog-3 above. We used a pulsed excitation signal at 440 nm and a repetition rate of 10 kHz, provided by a NanoLED-440LH (100 ps, FWHM), while detection was collected on the same TBX detector above. The fluorescence decay profile of the NCs (limited to a narrow window at the peak of the PL spectrum) was fitted to a mono-exponential decay function:

$$I(t) = I(0) \times \exp\left(-\frac{t}{\tau}\right) \quad (2)$$

where t is time, $I(0)$ is the PL intensity at t = 0, and τ is the excited state lifetime.

The ^{1}H NMR spectra were collected using a Bruker Spectro-Spin 600 MHz spectrometer (Billerica, MA). FT-IR spectra were measured on a PerkinElmer FT-IR spectrometer. The high angle annular dark field scanning transmission electron microscopy (HAADF-STEM) imaging was carried out on a probe-aberration-corrected JEOL JEM-ARM200cF with a cold-field emission gun at 200 kV. The STEM resolution of the microscope is 0.78 Å. The HAADF-STEM images were collected with a JEOL HAADF detector using the following experimental conditions: probe size 0.78 nm, scan speed 32 μs per pixel, and camera length 8 cm, which corresponds to a probe convergence angle of 21 mrad and inner collection angle of 76 mrad. The energy dispersive X-ray spectroscopy (EDS) maps were collected in the STEM mode with a probe size of 0.11 nm using Oxford Aztec EDS detector.

The X-ray photoelectron spectroscopy measurements were carried out using PHI 5100 series instrument from PHI Inc. (Chanhassen, MN), equipped with a unmonochromated Mg Kα source (1253.6 eV) with the pass energy of the analyzer maintained at 89.45 eV. The photoelectron take-off angle was 45° relative to the sample surface. The binding energy (BE) scale of the system was calibrated using the values for $Au4f_{7/2}$ = 83.8 eV and $Ag3d_{5/2}$ = 368 eV. The samples were drop cast on freshly deposited graphite coated stubs under dry nitrogen flow. The collected spectra were an average over 15 sweeps using 0.05 eV steps and 500 ms dwell times. The base pressure of the UHV analysis chamber was maintained at $\sim 6 \times 10^{-10}$ mbar. A Shirley background was subtracted from all spectra and the peaks were fit to a Gaussian–Lorentzian function.

Synthesis of $[Au_{11}(PPh_3)_8Cl_2]^+$. The triphenylphosphine-protected Au_{11} clusters (which served as precursors for growing the nanocluster cores) were prepared following literature methods, but in a rather small scale.[20,23] Briefly, 0.025 mmol $HAuCl_4 \cdot 3H_2O$ (0.1 mL of solution, 0.1 g mL^{-1}), was dissolved in 1 mL of ethanol, then 19.9 mg of triphenylphosphine (0.076 mmol) was added. The mixture was sonicated for 1 minute, which resulted in a curdy white precipitate of gold–phosphine complexes. A small magnetic bar was introduced, and then a solution of $NaBH_4$ in ethanol (250 μL, 9.6 mg mL^{-1}, *i.e.*, 0.063 mmol) was added dropwise to the mixture over $\sim$1 min. The solution turned dark brown immediately and was left stirring for 2 hours. The solvent was evaporated using a rotary-evaporator (without heating) and the dry product was washed two times with hexane, to remove excess phosphine ligands, followed by washing twice with DI water to remove inorganic impurities. The residual product was dissolved in ethanol (1 mL) and directly used in the next step to grow the bimetallic NCs. A new batch of Au_{11} clusters was freshly prepared every time before the growth of Au/Ag nanoclusters.

Ligand synthesis. Details on the synthesis of the various monothiol-appended ligands, including acetyl-protection, coupling to PEG blocks and zwitterion groups and thiol deprotection are provided in the ESI.†

Synthesis of Ag(I)–SR complex. The silver complexes with aliphatic thiols were prepared as described in the literature.[23] Briefly, 0.05 mmol of $AgNO_3$ and 0.05 mmol of thiol ligands (equimolar amounts) were dissolved in ethanol (1 mL) along with triethylamine (20 μL) at room temperature, which yielded a light yellow precipitate. The precipitate was washed several times with ethanol and dried under vacuum to obtain the pure Ag(I)–SR complex. The dried complex was stored until further use. Conversely, silver–thiolate complexes of PEG/zwitterion-modified ligands were prepared by mixing equimolar amounts of Ag(I) precursor with the PEG/zwitterion thiol ligands. The solution immediately became light yellow, indicating the formation of Ag(I)–S-PEG complex. The Ag(I)–S-PEG complex was prepared in ethanol while the Ag(I)–S-zwitterion complex was prepared in methanol, because the zwitterionic ligand was not readily soluble in ethanol. This solution was used as prepared for the growth of Au/Ag nanoclusters. Assuming that the complex formation is 100% efficient, the amount of the silver–thiolate complex was varied between 2 and 0.25 molar equivalent with respect to the gold precursor initially used for the preparation of Au_{11} clusters. For the optimized conditions, 0.0063 mmol $AgNO_3$ (126 μL, 50 mM) was added to an equivalent molar amount of the monothiol PEG/zwitterion ligand in 1 mL ethanol/methanol. The mixture was stirred for 1 hour and used in the next step for the growth of Au/Ag NCs.

Growth of hydrophobic Au/Ag nanoclusters. The hydrophobic Au/Ag NCs were prepared by reacting the phosphinated Au_{11} nanoclusters with the Ag(I)–SR complex described above.[23] Our purification scheme was slightly different from those described in the literature,[23] though. Instead of passing the prepared clusters through sephadex LH20 column, we precipitated the insoluble by-products by centrifugation, collecting the green supernatant, which was further passed through a 0.45 μm PTFE

syringe filter (Millipore). The NC dispersions were stored as collected at 4 °C in ethanol until further use.

Growth of hydrophilic Au/Ag nanoclusters. To grow the PEG- or zwitterion-capped NCs the Ag(I)–thiolate–PEG (or Ag(I)–thiolate–zwitterion) complex was added dropwise to the Au_{11} cluster solution (in ethanol or methanol) at room temperature while stirring. The mixture immediately changed color from reddish brown to dark brown. After additional stirring for ~6 hours, the content turned dark green and generated bright red emission under UV excitation. An additional 15–20 mg of free ligands were added to the vial and the mixture was further stirred overnight; this ensures sufficient coverage on the nanocluster surfaces with thiolate ligands.[42] We should note that due to the limited solubility of the zwitterion motif in ethanol, NC growth using the Ag(I)–thiolate–zwitterion complex was carried out in a mixture of ethanol/methanol at 40 °C. The reaction was left to proceed for three hours, then excess zwitterion ligand was added, and the mixture was stirred overnight at 40 °C. Once the reaction was complete, insoluble residues were removed by precipitation/centrifugation and then filtration. The clear nanocluster dispersion was purged with nitrogen and then stored as prepared in ethanol at 4 °C until further use. To disperse the nanoclusters in aqueous solution, an aliquot of the stock dispersion was retrieved in a separate vial and the solvent was evaporated. To remove excess PPh_3 ligand, the dry product was washed with hexane two times using sonication. After removal of hexane (using a pipette), the nanoclusters were dried under vacuum and dispersed in 0.5 mL of DI water. Functionalization of the NCs was achieved by growing the NCs in the presence of $-N_3$, $-NH_2$ or –COOH-terminated thiol–PEG ligands. Nonetheless, due to the limited solubility of the PEG–azide ligands, the growth was carried out using a 50 : 50 molar mixture of thiol–PEG_{750}–OCH_3 : thiol–PEG_{600}–N_3.

Results and discussion

Our approach builds on several recent developments reporting the growth of well-characterized noble metal nanoclusters, with enhanced fluorescence properties.[16,17,23,28,43–45] For instance, Jin and coworkers showed that reaction of triphenylphosphine-capped undecagold clusters with silver–thiolate complexes yielded highly luminescent alloyed core nanoclusters with the composition of $[Au_{25-x}Ag_x(PPh_3)_{10}(SR)_5Cl_2]^{2+}$.[23] These bimetallic core materials are substantially more fluorescing than Au_{25} NC counterparts. This result along with others have motivated researchers to adapt these nanoclusters for developing fluorescence-based applications such as imaging probes in biology. One potentially effective approach is to adapt the above growth route using Ag(I)–thiolates made with ligands that present a hydrophilic motif. To achieve this, we synthesized a set of ligands that present either a PEG block or a zwitterion group appended onto an undecanethiol molecule; the latter promotes coordination onto the nanocluster surfaces. The synthetic steps and chemical structures of the various ligands used in this study are schematically represented in Fig. 1 and 2. Additional details are provided in the ESI.† Below we describe the growth of fluorescent NCs carried out by combining three complementary steps: (i) synthesis of the phosphinated undecagold clusters (Au_{11}) as described in ref. 20 and 46; (ii) formation of the Ag(I)–SR (where R = $-C_{12}$, $-C_{11}$–PEG–X or $-C_{11}$–zwitterion); and (iii) growth of the bimetallic Au/Ag nanoclusters. Growth of NCs in the presence of hydrophobic ligands, presenting varying alkyl chains, provides control samples and allows easy comparison with the materials described in ref. 23 and 47.

To prepare the Au_{11} clusters, Au(I)–PPh_3 complex was first prepared by reacting $HAuCl_4$ with triphenylphosphine. The resulting insoluble complex was then chemically reduced using $NaBH_4$ in ethanol to yield a solution of precise composition clusters, $[Au_{11}(PPh_3)_8Cl_2]^+$, which appears reddish brown and exhibits a characteristic absorption peak at ~415 nm; an absorption spectrum of a dispersion of Au_{11} clusters is provided in the ESI† (Fig. S2).[46] Growth of the bimetallic Au/Ag NCs was carried out by reacting the Au_{11} clusters (serving as precursors) with Ag(I)–thiolate complexes in ethanol; no reducing agent is required for this step.

Fig. 2B shows representative profiles of the optical absorption, PL excitation and PL emission collected from a dispersion of dodecanethiol-protected Au/Ag NCs. Materials with similar properties were also grown using the other hydrophobic ligands including hexanethiol, propanethiol and mercaptopropionic acid (data not shown). The optical absorption spectrum in Fig. 2B shows absorbance features at 655 nm, 487 nm, 425 nm, 370 nm and 330 nm. Similarly, a representative PL excitation scan collected using a detection at the maximum emission wavelength (here ~760 nm) shows well-defined features that are consistent with those measured in the absorption profile (see Fig. 2B). Conversely, the PL spectra collected from these dispersions exhibit the same profiles, with a maximum at ~760 nm, regardless of the excitation wavelength used. Only the PL intensity changed, depending on the optical density (OD) at the excitation line; a similar result is observed for the NCs grown in the presence of PEGylated thiolate ligands (see data below). This behavior indicates that the PL is generated from homogeneous NCs, in agreement with the data reported in Fig. 2 of ref. 23. Similar to the $[Au_{25-x}Ag_x(PPh_3)_{10}(SR)_5Cl_2]^{2+}$ nanoclusters reported by Jin and coworkers and Xia and co-workers in ref. 23 and 47, our absorbance and excitation profiles show a few key features spanning the wavelengths from the red to the blue regions of the spectrum. The exact locations of the peaks do not fully match those reported in the above references, nonetheless. For instance, the spectra in panel Fig. 2B show five distinguishable excitation features at 655 nm, 487 nm, 425 nm, 370 nm and 330 nm, compared to essentially three major features at 640 nm, 425 nm, 370 nm reported in ref. 23 and 47. The PL peak position is different from the one reported by Jin's group (peak at 670 nm) in ref. 23, but closer to the one reported by Xia's group (peak at 720 nm) in ref. 47, and essentially identical to the one recently reported for the same NCs in ref. 48. The absolute PL quantum yield measured (~40%) is comparable to the one reported in ref. 23.

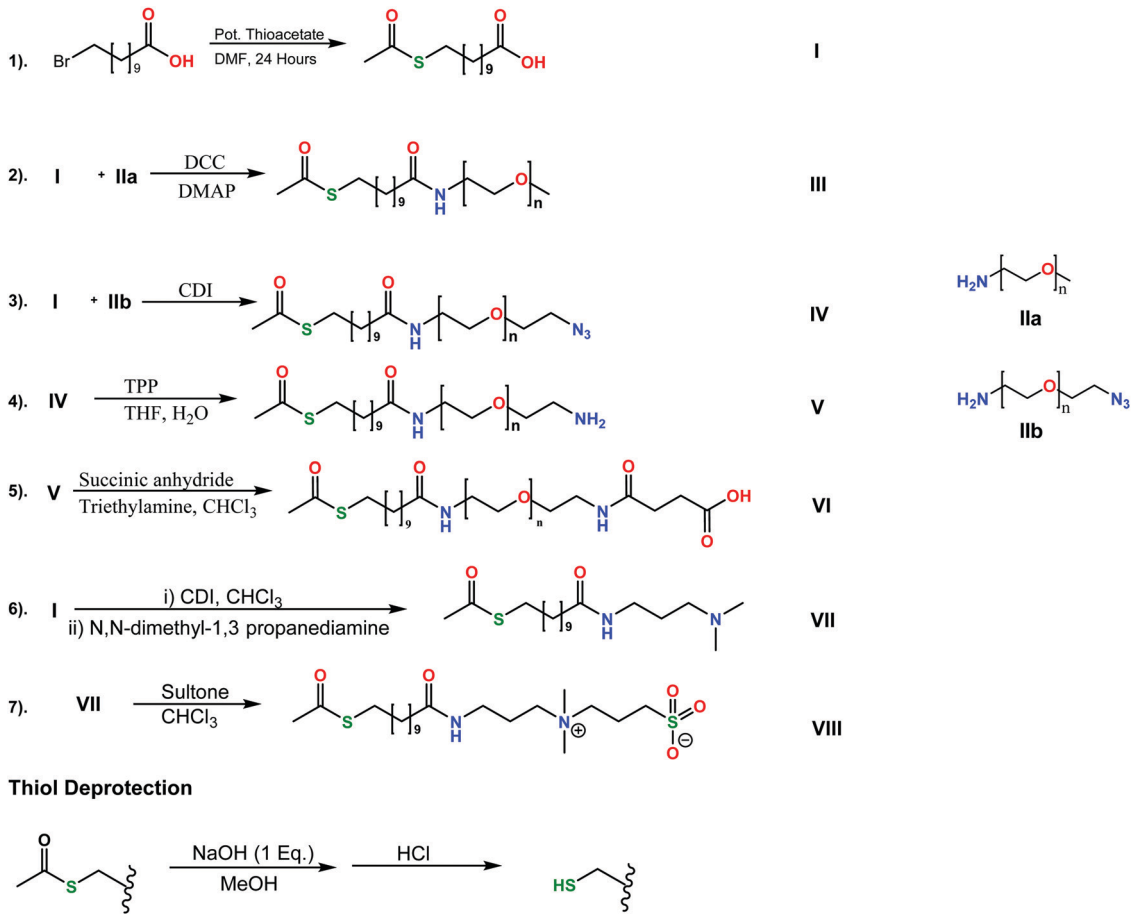

Fig. 1 Schematic representation of the reaction steps and reagents used in the synthesis of the various thiol-modified ligands.

The time-resolved fluorescence decay profile collected from the hydrophobic dodecanethiol-protected nanoclusters in ethanol is shown in Fig. 2C. The decay profile was fitted to a mono-exponential decay function (eqn (2)), yielding an average lifetime of ~12.7 μs. This value is longer than that measured for Au or Au-doped Ag NCs reported by a few groups including ours (~1–2 μs).[32,49,50] The above value is, however, comparable to that reported for phenyl ethanethiol-protected $Au_{25-x}Ag_x$ nanoclusters characterized by Xia and co-workers, who reported a PL lifetime of 7.4 μs.[47]

Given the high fluorescence of the bimetallic NCs grown using the hydrophobic ligands, we reasoned that applying the same strategy to grow hydrophilic Au/Ag NCs using thiol–PEG–X ligands that present different terminal functionalities could yield materials with promising spectroscopic properties (NIR emission and high QY) and potentially applicable in biology. The introduction of new ligands with additional properties (*e.g.*, PEGylated or zwitterion thiolate ligands in the present case) is carried *in situ* during the growth reaction, as done for AuNPs.[42] This approach is different from the one achieved *via* ligand exchange, reported by Murray and co-workers.[51] However, our initial attempts to grow PEG- or zwitterion-stabilized nanoclusters using the parameters to grow the hydrophobic NCs (namely in terms of reagent concentrations described above) yielded materials with practically insignificant emission. Inspired by our recent study showing that the PL properties of hybrid core Au/Ag NCs, capped with lipoic acid derivatives, are strongly dependent on the Au-to-Ag ratio used, we tested the effects of varying the molar concentration of the Ag(I)–thiolate–PEG complex added during NC growth (in step iii, above).[32] More precisely, we varied the molar ratio (mol. eq.) of Ag(I)-complex to Au(III) precursor used in the preparation of the Au_{11} clusters from 2 to 0.25. The progression of the absorbance, excitation and PL profiles with the changes in the mol. eq. of Ag(I)–thiolate–PEG complex are summarized in Fig. 3. Data show that addition of higher concentration of the complex (*i.e.*, 2 or 1 mol. eq. of Ag(I)–thiolate–PEG) immediately produced a dark brown solution, with absorbance that steadily increased with decreasing wavelengths below 650 nm and the appearance of broad absorption feature around 475 nm. Additionally, these materials exhibited very weak PL. When the amount of Ag(I)-complex was lowered to 0.5 mol. eq., a greenish-brown solution was formed, and the corresponding absorption spectrum showed broad features spanning the range 350–660 nm. A non-negligible PL signal was measured. Furthermore, decreasing the mol. eq. of Ag(I)–thiolate–PEG–OCH_3 complex to 0.25 produced a brown-green solution and the collected absorption spectrum exhibited features similar to those shown in Fig. 2B,

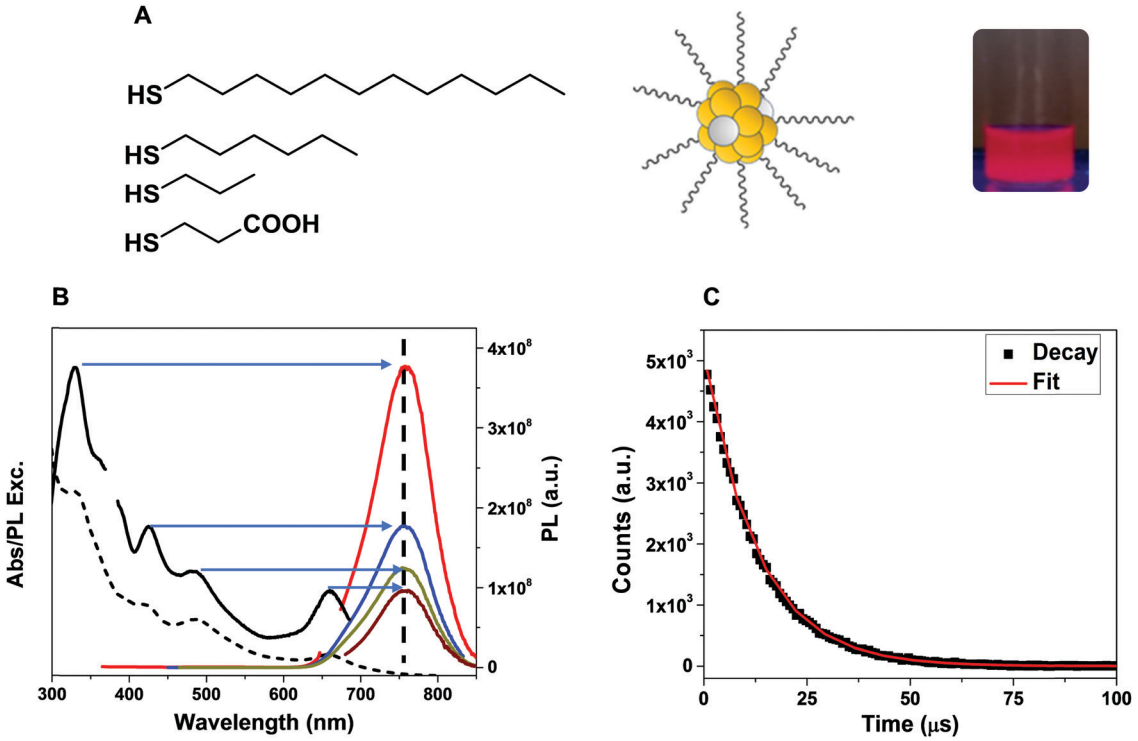

Fig. 2 (A) Schematic representation of bimetallic NC capped with monothiol–alkyl ligands. Four alkyl–thiol ligands with various chain lengths are shown. The fluorescence image is collected from a dispersion of dodecanethiol-protected NCs in ethanol irradiated using a hand-held UV lamp. (B) Absorption profile (black dashed line), PL excitation scan (black solid) and excitation-dependent PL emission spectra of the same nanoclusters. (C) Time-resolved decay profile collected from a dispersion of the nanoclusters in ethanol; excitation at 485 nm. We should note that the experimental data points around 650–670 nm in the red PL profile and around 370 nm in the excitation spectrum (both in B) have been discarded as they coincide with contribution of the second overtone from the excitation at 330 nm and *vice versa*.

combined with a strong emission centered at ~730 nm. We thus set the mol. equivalent of Ag(I)–thiolate–PEG–X, relative to the amount of gold precursor initially used for preparing Au_{11} clusters, to 0.25 and applied all analyses to NCs acquired using this condition.

The optical absorption and PL excitation spectra of the nanoclusters prepared starting with Ag(I)–thiolate–PEG–OCH_3, shown in Fig. 4A, have overall the same excitation features measured for the dodecanethiol-protected Au/Ag NCs shown in Fig. 2, though slightly shifted; the features are at 642, 472, 425, 370, and 325 nm. Furthermore, the time-resolved decay profiles collected from the thiol–PEG–OCH_3-protected NCs were also fit to single exponential decay function with a lifetime of ~8 μs, which is slightly smaller than that measured for the dodecanethiol-protected NCs. We infer from the data that the two sets of nanoclusters (hydrophobic NCs shown in Fig. 2 and PEGylated NCs shown in Fig. 4) have similar core size, though the exact stoichiometry may differ; for instance the molar fraction of Ag(I)–thiolate precursors used for the PEGylated compound was ~8 times smaller than those grown using dodecanethiol. Additionally, the NMR spectrum of the PD10 purified nanoclusters (shown in Fig. 4C) confirms the presence of both triphenylphosphine and PEG thiolate ligands on the NC surfaces, with approximate PPh_3 to thiolate ratio of 1.2 : 1. We should note that treatment with excess of thiol–PEG ligand overnight did not lead to complete displacement of PPh_3 ligands from the nanocluster surfaces.

Further characterization of the NC size, structure and composition of the PEGylated materials (as a representative set) was carried out using HAADF-STEM, EDS and XPS measurements. The TEM images (in Fig. 5, panels A, B, C) clearly show that the as-prepared samples are made of mixtures of small size nanostructures, with an average core size of ~0.95 ± 0.25 nm. Some of the larger size nanocrystals (1–2 nm diameter) present crystal arrangement of the atoms, which is indicative of small metal nanoparticles. However, if we focus on the smaller sub-set of those nanostructures we can identify several anisotropic nanocrystals (some of them are outlined with the red dashed ellipsoids) with varying spatial orientation on the TEM grid (see Fig. 5B and C). Combined with the absence of any crystal planes, these nanostructures can be identified as 25-metal atom core nanoclusters. Their concentration is large enough to impart the appearance of a few key absorption features in the measured absorption and excitation spectra, as shown in Fig. 4. We note that 1–2 nm nanoparticles tend to exhibit featureless absorption spectra,[42] which superpose on the profiles of the nanoclusters yielding the data shown in Fig. 2–4. The EDS element map shows an even distribution of Au and Ag, see Fig. 5D. Furthermore, analysis of the various integrated peak intensities in the EDS spectrum (Fig. 5E) has provided an estimate for the NC core stoichiometry, with an average Au : Ag ratio of ~4 : 1, in agreement with the stoichiometry of the starting Au and Ag precursors (0.25 eq. of Ag(I)–thiolates).

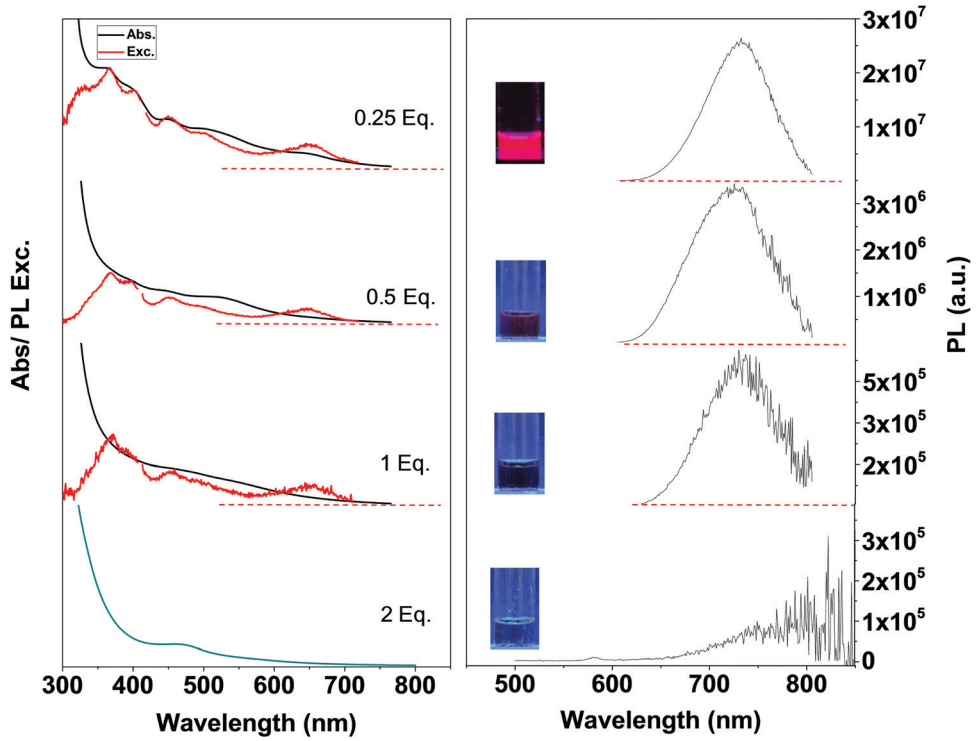

Fig. 3 Effect of varying the concentration of Ag(I)–S-PEG–OCH_3 complex used during the growth conditions (reported as mol. eq.) on the optical properties of the resulting bimetallic nanoclusters. The mol. eq. values were taken with respect to the amount of gold precursor ($HAuCl_4 \cdot 3H_2O$) used in the preparation of Au_{11} clusters.

Fig. 5, panels F and G show the XPS spectra of the same PEGylated NCs corresponding to Au4f and Ag3d regions. The $Au4f_{7/2}$ peak for Au and the $Ag3d_{5/2}$ peak for Ag atoms (represented by blue vertical line) were found at 85 eV and 368.5 eV, respectively. Both values are slightly higher than those measured for metallic Au(0) ($\sim$84 eV) and Ag(0) ($\sim$368 eV), which confirm the rather small size of the prepared NCs and that a fraction of those atoms are coordinated to thiolate ligands.[24,32,52,53] The rather noisy spectrum of the silver shown in panel G may be due to the smaller concentration of Ag atoms in the NC compared to Au, as inferred from the EDS data above. We would like to note that we have not been able to collect reliable mass spectroscopy data from our NC materials. This problem can be attributed to the nature of the coating, as long alkyl chains or PEG blocks tend to be greasy, making optimal sample preparation complex. Additionally, the inherent polydispersity of PEG chains renders the generation of exploitable mass spectra difficult.[12]

The growth strategy described above can also be used to introduce azide, amine, and carboxy functionalities on the nanocluster surfaces. This is achieved by simply starting with HS-PEG–X (X = $-N_3$, $-NH_2$, or –COOH) ligand to form the Ag(I)–thiolate–PEG–X complexes, followed by reaction with Au_{11} clusters as described above. We should note that since 100% azide-functionalized nanoclusters were not readily soluble in water, we used a 50 : 50 molar mixture of $-N_3$ and $-OCH_3$ during the overnight reaction (*i.e.*, growth combined with the surface passivation step). The optical absorption and emission profiles of these surface-functionalized NCs (see Fig. S3, ESI†) are overall comparable to those measured for the nanoclusters capped with HS-$C_{11}H_{23}$ and HS-PEG–OCH_3 ligands, shown above in Fig. 2 and 4. The presence of the azide groups on the purified nanocluster surfaces was confirmed by IR spectroscopy (Fig. S4, ESI†). The cluster sample showed a peak around 2090–2100 cm^{-1} (red curve) corresponding to the azide group, which resembles the peak measured for the pure ligand (black curve). Characterizing the stoichiometry of $-NH_2$/–COOH/$-N_3$ *vs.* $-OCH_3$ in mixed ligand coating using NMR spectroscopy is difficult, because of the weak ^1H NMR signatures of $-NH_2$ and –COOH. However, we know from previous experiments, using absorption and fluorescence measurements that cap exchange applied to already formed NCs, or growth of the NCs using mixed ligands produce materials where the ligand stoichiometry in the coating is preserved.[54,55] Thus, we anticipate that for the NCs grown using PEG–NH_2 or PEG–COOH would yield the ligand stoichiometry reported in Fig. 4, with PPh_3 : PEG–NH_2/COOH = $\sim$1 : 1. That ratio will be smaller for the growth performed in the presence of PEG–N_3. Since a 50 : 50 mixture of HS-PEG–OCH_3 and HS-PEG–N_3 was used, the surface stoichiometry will be PPh_3 : HS-PEG–OCH_3 : HS-PEG–N_3 = 1 : 0.5 : 0.5 in the final product.

The as-prepared nanoclusters grown using alkyl–thiolate, PEG–thiolate and zwitterion–thiolate stay dispersed in organic solutions (*e.g.*, ethanol) and fluorescent for several months (at least 6 months). The nanoclusters also maintain their fluorescent properties for a long period of time when stored dry. Nonetheless, the zwitterion-coated NCs tend to become jelly materials when dried, but maintain their fluorescence properties. The NCs

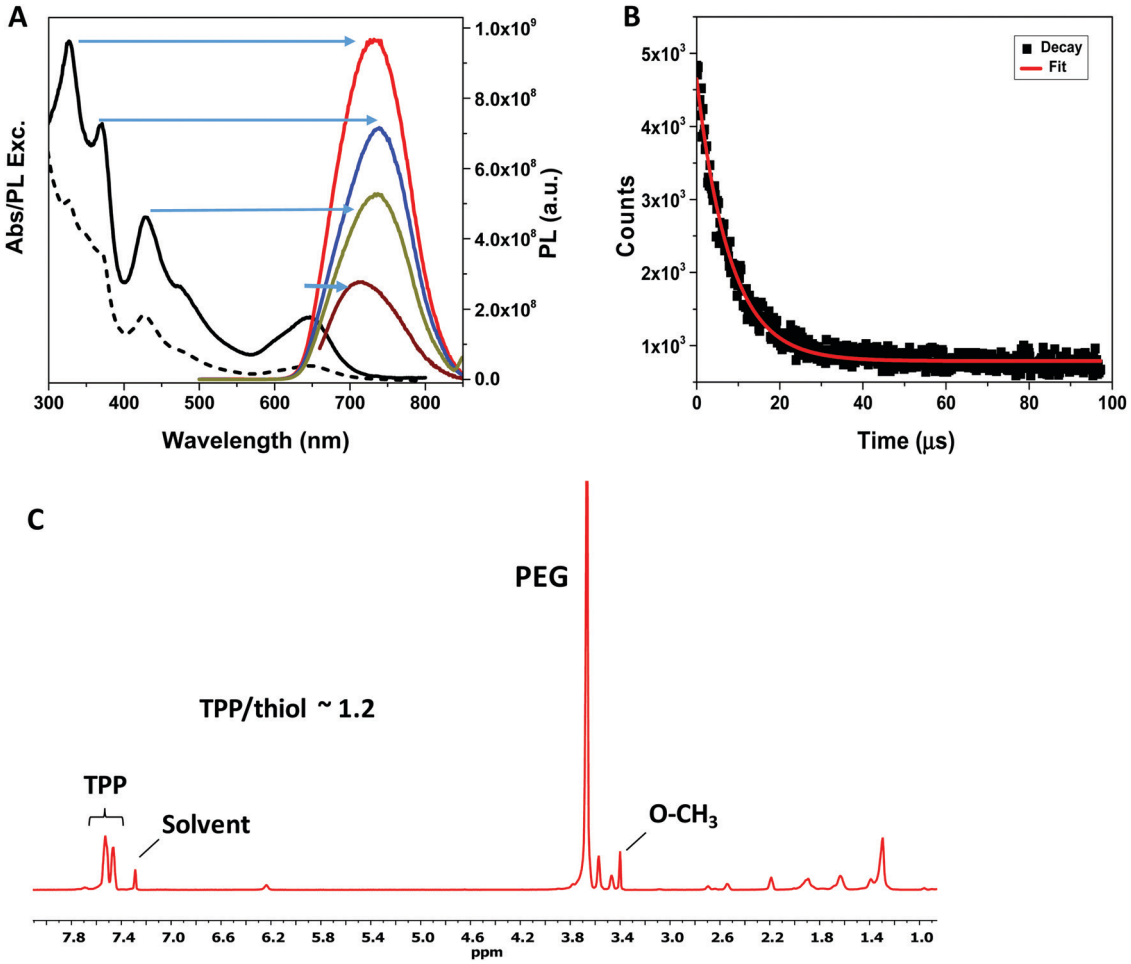

Fig. 4 (A) PL excitation scan (black solid line) along with the absorbance spectrum of the NCs (black dashed line). Also shown are the excitation-dependent PL emission spectra of the thiol–PEG–methoxy-protected Au/Ag nanoclusters. (B) Time-resolved PL decay curve collected from the nanoclusters in water, using an excitation at 440 nm. (C) ^{1}H NMR spectrum of the pure cluster sample dried and then redispersed in $CDCl_3$.

grown using PEG and zwitterion ligands can be transferred to aqueous media, which can be realized *via* evaporation of the organic solvent then redispersion in water. However, we found that the integrity of NCs along with their photophysical properties are best preserved if the dried NCs were initially dispersed in acidic solution (HCl, pH 3), then purified using the following steps: first 2–3 rounds of concentration/dilution are applied using membrane filtration device (MW cutoff = 10 kDa, from Millipore), to remove excess ligands. The dispersion is then passed through a PD10 column. Both purification steps are carried using the same acidic solution (pH 3). Fig. 6A shows fluorescence images collected, over the period of ~2 months, from dispersions of PEGylated-NCs in PBS buffer (pH 3, 7, 11). The excitation and PL emission spectra monitored over the same period are essentially unchanged. The results combined clearly show that these hydrophilic materials stay colloidally stable over the pH 3–11 range for extended period of time (several months). We attribute the improved long term colloidal and photophysical stability of the hydrophilic NCs to the beneficial effects of introducing chlorides into the sample during the phase transfer step, which are anticipated to provide additional surface coordinating species, further enhancing the steric stability and preserving the absorption and PL features, as shown in Fig. 6. Additional excitation and fluorescence spectra collected from the NC dispersions at pH 7 and pH 11, over the same storage period, are shown in the Fig. S5 (ESI†). These spectra indicate that under basic buffer conditions there is a slow but progressive decay in the PL excitation and emission spectra, which is more pronounced than what was measured at pH 3 (shown in Fig. 6). This may attributed to the presence of higher concentration of OH^- ions at those pH values, which reduces the stabilizing effects of Cl^- ions in the medium.

Finally, we would like to discuss our data in comparison to other materials described in the literature, with a focus on bimetallic Au/Ag and pure Au 25-atom core nanoclusters, and to theoretical predictions. Though we were not able to generate reliable mass spectroscopy data, we discuss our fluorescent materials within the context of well-defined core structure. The nanoclusters prepared in this work (namely, the subset of grown cores identified as nanoclusters in Fig. 5) yield absorption spectra that exhibit well defined features (five), along with an absorption onset that is blue shifted compared to the profile

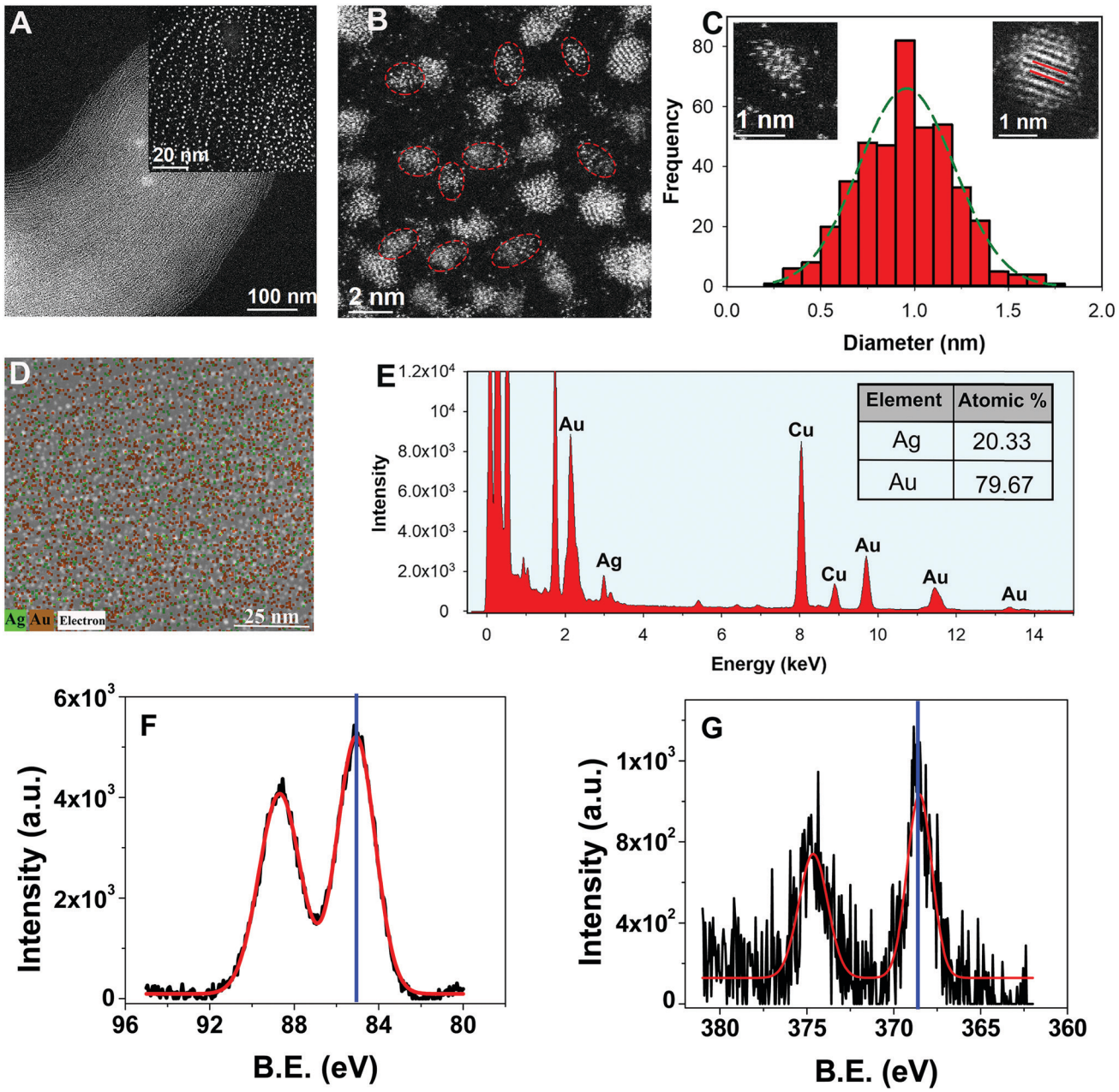

Fig. 5 (A) Low magnification TEM image of Au/Ag nanoclusters grown with monothiol–PEG–OCH_3 ligands. Sample was purified first, followed by processing from dispersion in water. (B) High magnification dark field image showing a smaller set of NCs. Structures identified as NCs are outlined with dashed red ellipsoids. (C) Histogram of the particle size distribution obtained using manual sizing approach, with average size = 0.95 ± 0.25 nm. TEM images of a single NC and a single NP are shown in the insets. (D) Energy-dispersive X-ray spectroscopy (EDS) mapping of NCs showing the co-distribution of Au and Ag. (E) EDS spectra of the NCs. The inserted table shows an experimental ratio of Au : Ag = 4 : 1. XPS spectra collected from a film of the Au/Ag NCs, focusing on the Au4f region (F) and the Ag3d region (G) of the energy spectrum.

measured for pure Au_{25} core materials shown in ref. 23, 47 and 56. Absorption data from Au cores with thiolate surface cap have been compared to predictions of the electronic structures developed using time-dependent density functional theory (TD-DFT) simulations.[13,14] Differences in the optical features of the grown NCs arise regardless of the structure of the Ag(I)–thiolate precursor used. We propose that the nanoclusters prepared in this study are essentially bimetallic Au/Ag cores made of 25 total atoms, capped with a mixture of PPh_3 and alkyl–thiolate, PEG–thiolate or zwitterion–thiolate ligands. Our proposal is based on the detailed spectral features in the absorption profiles combined with the pronounced PL properties, shown in Fig. 2, 3, and 6. The presence of Ag atoms in the cores is crucial for promoting the creation of charge carrier pairs (exciton) and the photoemission generated following recombination of those excitons. The PL enhancement of the Ag-containing NCs compared to pure Au core samples along with the QY measured for our NCs are similar to those reported in ref. 23 and 47.

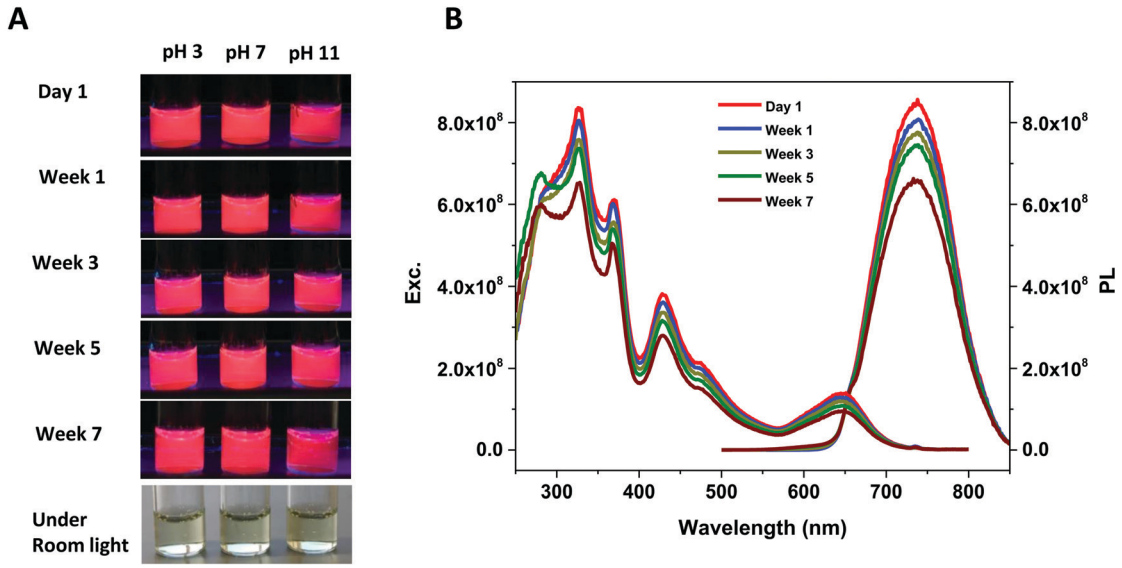

Fig. 6 Colloidal stability of methoxy–PEG–thiol-capped NCs. (A) Images of NC dispersions in different pH buffers irradiated with a hand held UV lamp (exc. at 365 nm) after 1, 3, 5 and 7 weeks of storage. White light image of the same set of dispersions after 4 weeks of storage. (B) Excitation and PL profiles collected from the NC dispersion (pH 3) at the conditions shown in panel A.

There are a few differences between our materials and those described in the works by Jin and Xia groups, nonetheless. The core composition of our emitting materials varies depending on the thiolate ligand used. The EDS and XPS data collected from the PEGylated NCs indicate that these bimetallic NCs have a smaller fraction of Ag atoms in their structures (Au : Ag $\sim$ 4 : 1 on average) than the highly emitting $Au_{12}Ag_{13}$ NCs described in the works of Jin and Xia. The NCs grown using alkyl thiolates may have closer composition to their materials, given that the fractions of Au and Ag in the starting precursors was closer to 1 : 2 (see Experimental details). The NIR PL emission with its rather long lifetime (8–12 μs) measured for our NCs is attributed to the dominance of metal to ligand charge transfer interactions, a phenomenon commonly observed for NCs stabilized by thiolate ligands.[47,49] As proposed by Xia and co-workers using TD-DFT calculations,[47] the appearance of well-defined and blue shifted absorption feature at the lowest energy level for $Au_{25-x}Ag_x$ NCs, prepared using this core transformation route (*e.g.*, peak at $\sim$642 nm in Fig. 4), is attributed to enlargement of the HOMO–LUMO gap by Ag doping at the central position of the anisotropic nanostructure. The PL enhancement measured for the bimetallic NCs also originates from the arrangement of the doping Ag atoms around the central plane of the rod-like NCs. Such enhancement is measured for the sets of NCs grown with either thiolate ligands. The difference in emission properties may be attributed to the different nature and size of the thiol ligands used. Phenylethanethiol is a short molecule appended with a benzene ring, whereas our ligands present either alkyl chains or alkyl–PEG/alkyl–zwitterion motifs. For instance, we note that the PL profiles generated by our bimetallic NCs grown in the presence of alkyl–thiolates and PEG–thiolate have peaks that are $\sim$30 nm apart, even though their absorption profiles are nearly identical. We and other groups have also measured different PL profiles for NCs grown in the presence of disulfide-presenting lipoic acid-based ligands.[12,24,32,57,58] Our growth route allows the transfer of the NCs to buffer media and yields hydrophilic dispersions that exhibit long term steric stability, while preserving high PL emission as shown in Fig. 6. This bodes well for potential applications in biological imaging and sensing.

We would like to conclude by noting that the low-magnification TEM image shown in Fig. 5A indicates the filamental arrangement of the PEGylated nanoclusters on the TEM grid that extends over distances much larger than a few micrometers. This is an interesting observation that merits additional investigation. Indeed, such filamental arrangement of NCs protected with *p*-MBA (*para*-mercaptobenzoic acid) and subjected to a cyclic dialysis in a pH gradient have been reported to generate PL enhancement of Au cores NCs, which are otherwise non luminescent when homogeneously dispersed in solution.[59] We will investigate the implication of the TEM data measured for our materials and hope to report on them in the future.

Conclusion

We have prepared and characterized a set of highly luminescent nanoclusters made of bimetallic cores. The growth route relied on the reaction of well-defined triphenylphosphine protected Au_{11} clusters with Ag(I)–thiolate complexes, which have been prepared using various thiol-appended ligands with differing structures and solubility properties. These ligands include commercially available alkyl thiol molecules, poly(ethylene glycol)- and zwitterion-appended undecanethiol compounds. The latter two sets of ligands were designed and prepared in our laboratory. This growth route consistently yielded nanoclusters with small size (diameter $\sim$1 nm) and bimetallic Au/Ag core composition. The optical properties of the nanoclusters, including

well-defined UV-vis absorption and PL excitation that resemble literature data, reporting the growth of $Au_{25-x}Ag_x$ nanoclusters. We also found that the reaction produces nanoclusters that exhibit NIR emission profiles with high quantum yields (QY $\sim$ 40% for both hydrophobic NCs and hydrophilic materials). The PEG- and zwitterion-capped NCs can further be prepared with surface functionalities (*e.g.*, azide, amine and carboxyl), making it easy to couple them to target molecules. Their small size combined with strong NIR emission, long PL lifetime, long term colloidal stability in water and convenient surface functionalization make them appealing for a variety of fluorescence imaging applications.

Conflicts of interest

Authors declare no conflict of interest.

Acknowledgements

The authors acknowledge the financial support from FSU, the National Science (NSF-CHE #1508501), the National Institutes of Health (NIH #R01 DC013080), AFOSR (Grant #FA9550-18-1-0144) and Asahi-Kasei Corp. for financial support. We also thank Prof. Ken Hanson (FSU) and his group for assistance with some of the time-resolved fluorescence measurements and Chengqi Zhang for assistance with the TEM imaging and NMR experiments. The TEM work was carried out at the FSU TEM facility, funded and supported by the Florida State University Research Foundation, the National High Magnetic Field Laboratory (DMR-1644779), and the State of Florida.

References

1 O. S. Wolfbeis, *Chem. Soc. Rev.*, 2015, **44**, 4743–4768.
2 R. Jin, C. Zeng, M. Zhou and Y. Chen, *Chem. Rev.*, 2016, **116**, 10346–10413.
3 B. O. Dabbousi, J. RodriguezViejo, F. V. Mikulec, J. R. Heine, H. Mattoussi, R. Ober, K. F. Jensen and M. G. Bawendi, *J. Phys. Chem. B*, 1997, **101**, 9463–9475.
4 H. Mattoussi, G. Palui and H. B. Na, *Adv. Drug Delivery Rev.*, 2012, **64**, 138–166.
5 K. D. Wegner and N. Hildebrandt, *Chem. Soc. Rev.*, 2015, **44**, 4792–4834.
6 H. Dong, S.-R. Du, X.-Y. Zheng, G.-M. Lyu, L.-D. Sun, L.-D. Li, P.-Z. Zhang, C. Zhang and C.-H. Yan, *Chem. Rev.*, 2015, **115**, 10725–10815.
7 H.-Q. Wen, H.-Y. Peng, K. Liu, M.-H. Bian, Y.-J. Xu, L. Dong, X. Yan, W.-P. Xu, W. Tao, J.-L. Shen, Y. Lu and H.-S. Qian, *ACS Appl. Mater. Interfaces*, 2017, **9**, 9226–9232.
8 L. Cao, X. Wang, M. J. Meziani, F. Lu, H. Wang, P. G. Luo, Y. Lin, B. A. Harruff, L. M. Veca, D. Murray, S.-Y. Xie and Y.-P. Sun, *J. Am. Chem. Soc.*, 2007, **129**, 11318–11319.
9 J. Li, X. Zhong, F. Cheng, J.-R. Zhang, L.-P. Jiang and J.-J. Zhu, *Anal. Chem.*, 2012, **84**, 4140–4146.
10 C.-A. J. Lin, T.-Y. Yang, C.-H. Lee, S. H. Huang, R. A. Sperling, M. Zanella, J. K. Li, J.-L. Shen, H.-H. Wang, H.-I. Yeh, W. J. Parak and W. H. Chang, *ACS Nano*, 2009, **3**, 395–401.
11 Y. Chen, D. M. Montana, H. Wei, J. M. Cordero, M. Schneider, X. Le Guével, O. Chen, O. T. Bruns and M. G. Bawendi, *Nano Lett.*, 2017, **17**, 6330–6334.
12 F. Aldeek, M. A. H. Muhammed, G. Palui, N. Zhan and H. Mattoussi, *ACS Nano*, 2013, **7**, 2509–2521.
13 D. Bain, S. Maity and A. Patra, *Phys. Chem. Chem. Phys.*, 2019, **21**, 5863–5881.
14 M. Zhu, C. M. Aikens, F. J. Hollander, G. C. Schatz and R. Jin, *J. Am. Chem. Soc.*, 2008, **130**, 5883–5885.
15 J. Zheng, C. Zhou, M. Yu and J. Liu, *Nanoscale*, 2012, **4**, 4073–4083.
16 J. Xie, Y. Zheng and J. Y. Ying, *J. Am. Chem. Soc.*, 2009, **131**, 888–889.
17 Z. Luo, X. Yuan, Y. Yu, Q. Zhang, D. T. Leong, J. Y. Lee and J. Xie, *J. Am. Chem. Soc.*, 2012, **134**, 16662–16670.
18 Y. Negishi, K. Nobusada and T. Tsukuda, *J. Am. Chem. Soc.*, 2005, **127**, 5261–5270.
19 B. Adhikari and A. Banerjee, *Chem. Mater.*, 2010, **22**, 4364–4371.
20 Y. Shichibu, Y. Negishi, T. Tsukuda and T. Teranishi, *J. Am. Chem. Soc.*, 2005, **127**, 13464–13465.
21 S. Wang, Y. Song, S. Jin, X. Liu, J. Zhang, Y. Pei, X. Meng, M. Chen, P. Li and M. Zhu, *J. Am. Chem. Soc.*, 2015, **137**, 4018–4021.
22 Y. Negishi, K. Munakata, W. Ohgake and K. Nobusada, *J. Phys. Chem. Lett.*, 2012, **3**, 2209–2214.
23 S. Wang, X. Meng, A. Das, T. Li, Y. Song, T. Cao, X. Zhu, M. Zhu and R. Jin, *Angew. Chem., Int. Ed.*, 2014, **53**, 2376–2380.
24 D. Mishra, F. Aldeek, E. Lochner, G. Palui, B. Zeng, S. Mackowski and H. Mattoussi, *Langmuir*, 2016, **32**, 6445–6458.
25 W.-Y. Chen, G.-Y. Lan and H.-T. Chang, *Anal. Chem.*, 2011, **83**, 9450–9455.
26 S. M. Copp, D. E. Schultz, S. Swasey and E. G. Gwinn, *ACS Nano*, 2015, **9**, 2303–2310.
27 C.-A. J. Lin, C.-H. Lee, J.-T. Hsieh, H.-H. Wang, J.-K. Li, J.-L. Shen, W.-H. Chan, H.-I. Yeh and W.-H. Chang, *J. Med. Biol. Eng.*, 2009, **29**, 276–283.
28 G. Soldan, M. A. Aljuhani, M. S. Bootharaju, L. G. AbdulHalim, M. R. Parida, A.-H. Emwas, O. F. Mohammed and O. M. Bakr, *Angew. Chem., Int. Ed.*, 2016, **55**, 5749–5753.
29 L. G. AbdulHalim, M. S. Bootharaju, Q. Tang, S. Del Gobbo, R. G. AbdulHalim, M. Eddaoudi, D.-e. Jiang and O. M. Bakr, *J. Am. Chem. Soc.*, 2015, **137**, 11970–11975.
30 X. Yuan, B. Zhang, Z. Luo, Q. Yao, D. T. Leong, N. Yan and J. Xie, *Angew. Chem., Int. Ed.*, 2014, **53**, 4623–4627.
31 X. Dou, X. Yuan, Q. Yao, Z. Luo, K. Zheng and J. Xie, *Chem. Commun.*, 2014, **50**, 7459–7462.
32 D. Mishra, V. Lobodin, C. Zhang, F. Aldeek, E. Lochner and H. Mattoussi, *Phys. Chem. Chem. Phys.*, 2018, **20**, 12992–13007.
33 B. K. Teo, *Polyhedron*, 1988, **7**, 2317–2320.
34 B. K. Teo and H. Zhang, *Proc. Natl. Acad. Sci. U. S. A.*, 1991, **88**, 5067–5071.

35 L. C. McKenzie, T. O. Zaikova and J. E. Hutchison, *J. Am. Chem. Soc.*, 2014, **136**, 13426–13435.
36 K. Susumu, B. C. Mei and H. Mattoussi, *Nat. Protoc.*, 2009, **4**, 424–436.
37 B. C. Mei, K. Susumu, I. L. Medintz and H. Mattoussi, *Nat. Protoc.*, 2009, **4**, 412–423.
38 B. C. Mei, K. Susumu, I. L. Medintz, J. B. Delehanty, T. J. Mountziaris and H. Mattoussi, *J. Mater. Chem.*, 2008, **18**, 4949–4958.
39 W. Wang, X. Ji, L. Du and H. Mattoussi, *J. Phys. Chem. C*, 2017, **121**, 22901–22913.
40 N. Zhan, G. Palui, M. Safi, X. Ji and H. Mattoussi, *J. Am. Chem. Soc.*, 2013, **135**, 13786–13795.
41 W. Wang, X. Ji, A. Kapur, C. Zhang and H. Mattoussi, *J. Am. Chem. Soc.*, 2015, **137**, 14158–14172.
42 E. Oh, K. Susumu, R. Goswami and H. Mattoussi, *Langmuir*, 2010, **26**, 7604–7613.
43 X. Yuan, Z. Luo, Q. Zhang, X. Zhang, Y. Zheng, J. Y. Lee and J. Xie, *ACS Nano*, 2011, **5**, 8800–8808.
44 Y. Yu, Z. Luo, D. M. Chevrier, D. T. Leong, P. Zhang, D.-E. Jiang and J. Xie, *J. Am. Chem. Soc.*, 2014, **136**, 1246–1249.
45 J. Liu, M. Yu, X. Ning, C. Zhou, S. Yang and J. Zheng, *Angew. Chem., Int. Ed.*, 2013, **52**, 12572–12576.
46 Y. Shichibu, Y. Negishi, T. Watanabe, N. K. Chaki, H. Kawaguchi and T. Tsukuda, *J. Phys. Chem. C*, 2007, **111**, 7845–7847.
47 M. Zhou, J. Zhong, S. Wang, Q. Guo, M. Zhu, Y. Pei and A. Xia, *J. Phys. Chem. C*, 2015, **119**, 18790–18797.
48 S. Chen, H. Ma, J. W. Padelford, W. Qinchen, W. Yu, S. Wang, M. Zhu and G. Wang, *J. Am. Chem. Soc.*, 2019, **141**, 9603–9609.
49 K. G. Stamplecoskie, Y.-S. Chen and P. V. Kamat, *J. Phys. Chem. C*, 2014, **118**, 1370–1376.
50 E. Porret, L. Sancey, A. Martín-Serrano, M. I. Montañez, R. Seeman, A. Yahia-Ammar, H. Okuno, F. Gomez, A. Ariza, N. Hildebrandt, J.-B. Fleury, J.-L. Coll and X. Le Guével, *Chem. Mater.*, 2017, **29**, 7497–7506.
51 R. Guo, Y. Song, G. Wang and R. W. Murray, *J. Am. Chem. Soc.*, 2005, **127**, 2752–2757.
52 D. Bain, S. Maity, B. Paramanik and A. Patra, *ACS Sustainable Chem. Eng.*, 2018, **6**, 2334–2343.
53 E. Oh, J. B. Delehanty, L. D. Field, A. J. Mäkinen, R. Goswami, A. L. Huston and I. L. Medintz, *Chem. Mater.*, 2016, **28**, 8676–8688.
54 N. Zhan, G. Palui, J.-P. Merkl and H. Mattoussi, *J. Am. Chem. Soc.*, 2016, **138**, 3190–3201.
55 E. Oh, K. Susumu, J. B. Blanco-Canosa, I. L. Medintz, P. E. Dawson and H. Mattoussi, *Small*, 2010, **6**, 1273–1278.
56 Z. Wu and R. Jin, *Nano Lett.*, 2010, **10**, 2568–2573.
57 L. Shang, N. Azadfar, F. Stockmar, W. Send, V. Trouillet, M. Bruns, D. Gerthsen and G. U. Nienhaus, *Small*, 2011, **7**, 2614–2620.
58 M. A. Muhammed, F. Aldeek, G. Palui, L. Trapiella-Alfonso and H. Mattoussi, *ACS Nano*, 2012, **6**, 8950–8961.
59 Z. Wu, Y. Du, J. Liu, Q. Yao, T. Chen, Y. Cao, H. Zhang and J. Xie, *Angew. Chem., Int. Ed.*, 2019, **58**, 8139–8144.

